Large-scale silver sulfide nanomesh membranes with ultrahigh flexibility

*Yuting Wang[1], Wei Li[1], Yanan Xu[2], Chenhui Han[1], Peng Meng[1], Cheng Yan[3], Dong-Chen Qi[1], Jingsan Xu[1]**

[1] *School of Chemistry and Physics and Centre for Materials Science, Queensland University of Technology, Brisbane, Queensland 4000, Australia*

[2] *Central Analytical Research Facility, Institute for Future Environments, Queensland University of Technology, Brisbane, Queensland 4000, Australia*

[3] *School of Mechanical, Medical and Process Engineering and Centre for Materials Science, Queensland University of Technology, Brisbane, QLD 4000, Australia*

**Corresponding author, Email: Jingsan.Xu@qut.edu.au*

Abstract: The growth of flexible semiconductor thin films and membranes is highly desirable for the fabrication of next-generation wearable devices. In this work, we have developed a one-step, surface tension-driven method for facile and scalable growth of silver sulfide (Ag_2S) membranes with a nanomesh structure. The nanomesh membrane can in principle reach infinite size but only limited by the reactor size, while the thickness is self-limited to ca. 50 nm. In particular, the membrane can be continuously regenerated at the water surface after being transferred for mechanical and electronic tests. The free-standing membrane demonstrates exceptional flexibility and strength, resulting from the nanomesh structure and the intrinsic plasticity of the Ag_2S ligaments, as revealed by robust manipulation, nanoindentation tests and *pseudo*-in-situ tensile test under scanning electron microscope. Bendable electronic resistance-switching devices are fabricated based on the nanomesh membrane.

Keywords: Flexible nanomesh, Nanoscale plasticity, Nanoindentation, In-situ tensile test, Resistance-switching device.

Inorganic semiconductor thin films play a key role in many optical and electrical devices such as transistors, light-emitting diodes, and solar cells. The conventional methods for the growth of thin films and membranes include chemical vapor deposition, physical vapor deposition, atomic layer deposition, and solution-based spin coating, etc.[1-3] Continuous and dense films can be obtained via these methods, but the films either have poor mechanical properties or are challenging for mechanical measurements.

Bulk inorganic semiconductor compounds are normally regarded as hard and brittle materials. But recently, several inorganic semiconductors with high ductility at room temperature were found, such as Ag_2S[4], ZnS (in darkness)[5], and InSe[6]. These findings have challenged the traditional recognition of plastic materials and promoted the discovery of new mechanisms for the ductility of bulk semiconductors. Take bulk α-Ag_2S as an example, which is an n-type semiconductor compound with a bandgap of 2 eV, is highly ductile, and can be readily processed to various shapes at room temperature. The ductility of α-Ag_2S is considered to arise from the weak Ag-S bond between the slip plane[4]. Flexible devices such as photodectors[7], non-volatile memory[1] based on α-Ag_2S membranes have been fabricated, whereas the mechanical properties of the material down to the nanoscale have not been explored yet.

In this work, we have developed a solution-based, self-assembling process for the growth of a large-scale, free-standing α-Ag_2S nanomesh membrane. The synthesis was simply executed by mixing the aqueous solutions of amidinothiourea (ADT) and $AgNO_3$ followed by standing for 24 h, which in principle can produce Ag_2S membranes with an infinite area at the water-air interface, but rather only limited by the size of the reaction container. Particularly, the membrane can be renewably formed at the interface after being transferred for mechanical and electrical tests. An ultra-high ratio of the lateral size and the thickness ($> 10^6$) is achieved for the membrane, comparable to that of single-atom layer materials such as graphene. Still,

the membrane is extremely flexible, expandable and deformable, which in part results from the nanomesh structure and in part from the intrinsic plasticity of the Ag_2S ligaments. Bendable electronic resistance switching devices are fabricated out of the nanomesh membrane.

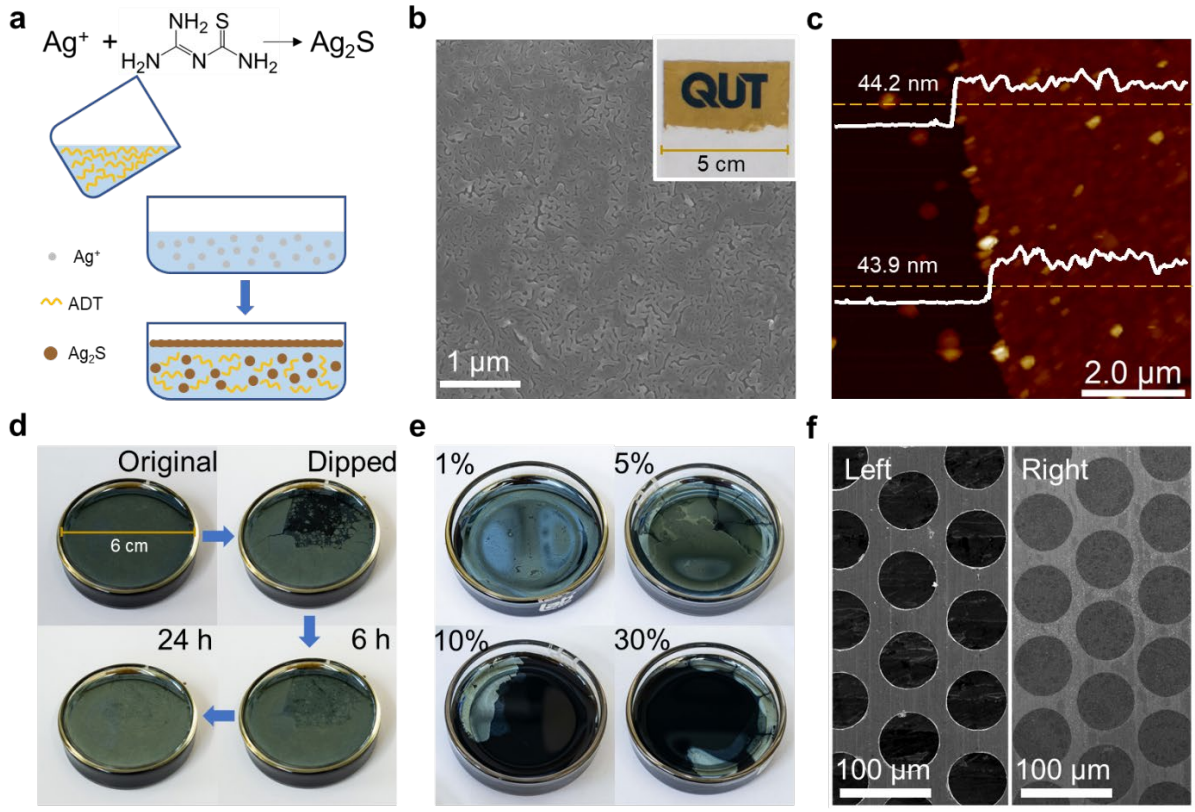

Figure 1. (a) Schematic illustration of the interfacial synthesis of Ag_2S membrane. (b) Top-view SEM image of Ag_2S membrane. Inset: membrane on a glass substrate. (c) AFM topography image and height profiles. (d) Photos of Ag_2S membrane on water for illustration of the regeneration process. (e) Ag_2S membrane on water with increased concentrations of ethanol in water. (f) Copper grid holes without (left) and with Ag_2S membrane (right) on top.

After mixing the aqueous solutions of $AgNO_3$ and amidinothiourea (ADT) in a petri dish, Ag_2S nanoparticles were immediately produced with the size of ca. 10 nm, forming a stable colloidal solution. It is worth mentioning that no extra stabilizing agent was used but rather ADT acted as a self-stabilizing molecule. Driven by the large surface tension of water, the nanoparticles floated onto the water-air interface where coalescence[8], and then a continuous Ag_2S membrane was formed on the water surface through oriented attachment (Figure S1)after

standing in dark for 24 h[9]. The two-dimensional growth of the membrane is only limited by the reaction container. Its size can readily exceed 10 cm^2 even after being transferred to a glass substrate (inset in Figure 1b, UV-vis spectrum shown in Figure S2). The powder X-ray diffraction (XRD) pattern confirms the formation of Ag_2S in the α-phase. Scanning electron microscopy (SEM) image (Figure 1b) reveals the nanomesh structure of the membrane on a silicon wafer (deposition method shown in Figure S3) and its thickness was determined to be 44 nm by atomic force microscopy (Figure 1c and Figure S4). As such, the lateral size/thickness ratio of the membrane reaches as high as 10^6, comparable to many atomic thick 2D materials such as graphene[10-11], MoS_2[12-14], and mica[15]. Very interestingly, the Ag_2S membrane can be continuously regenerated. As a demonstration, a part of the membrane was dipped out by a piece of glass, and then the void can be covered again by the newly formed Ag_2S on the surface, turning into a complete membrane after another 24 h standing (Figure 1d). This regeneration process can repeat many times until the Ag_2S concentration was not high enough.

To investigate the effect of surface tension on membrane growth, ethanol was added to the aqueous solution for lowering the surface tension. The membrane was still formed at relatively low ethanol concentrations (1 and 5 vol%), but with poor integrity (Figure 1e). When the surface tension was further decreased with more ethanol added (10 and 30 vol%), the membrane only appeared at the edge of the petri dish. This phenomenon can be explained by the Young-Laplace equation $\Delta p=2\gamma/r$, where Δp is Laplace pressure, γ is the surface tension, and r is the radius of curvature: the concave surface at the edge endows outward Laplace pressure on the Ag_2S nanoparticles, which provides an extra driving force for the membrane formation at the water-air interface. More discussion about the effect of surface properties on membrane growth is provided in the supplementary information (Figure S5-S7).

The Ag_2S nanomesh membrane can self-supportively stand across large holes, as displayed by the SEM images of the grid in which with and without the Ag_2S membrane on

top are compared (Figure 1f). In this circumstance, pretension is considered to exist within the membrane as reflected by the expanded mesh: the density of the ligaments located on the edge of the grid hole is much lower than that located in the center (Figure 2a, b). The widths of the blank areas along the vertical and horizontal directions are then measured and recorded (Figure 2c): the width in the center of the hole is concentrated at 60 nm, which is very similar to that of Ag_2S membrane deposited on carbon film (Figure S8), while the width on the edge is larger and more dispersed, ranging from 60 to 400 nm. These results demonstrate that the partially dissipated pretension *via* pore expansion should be one of the mechanisms that contribute to the flexibility of the membrane with great connectivity (Figure S9). Further, we noticed that the crystallinity of the ligament may be destroyed under such high stress. One typical spot is shown in Figure 2d, where clear lattice fringes were observed above the yellow dashed line, while at the waist of the ligament the structure becomes disordered due to the stress concentration.

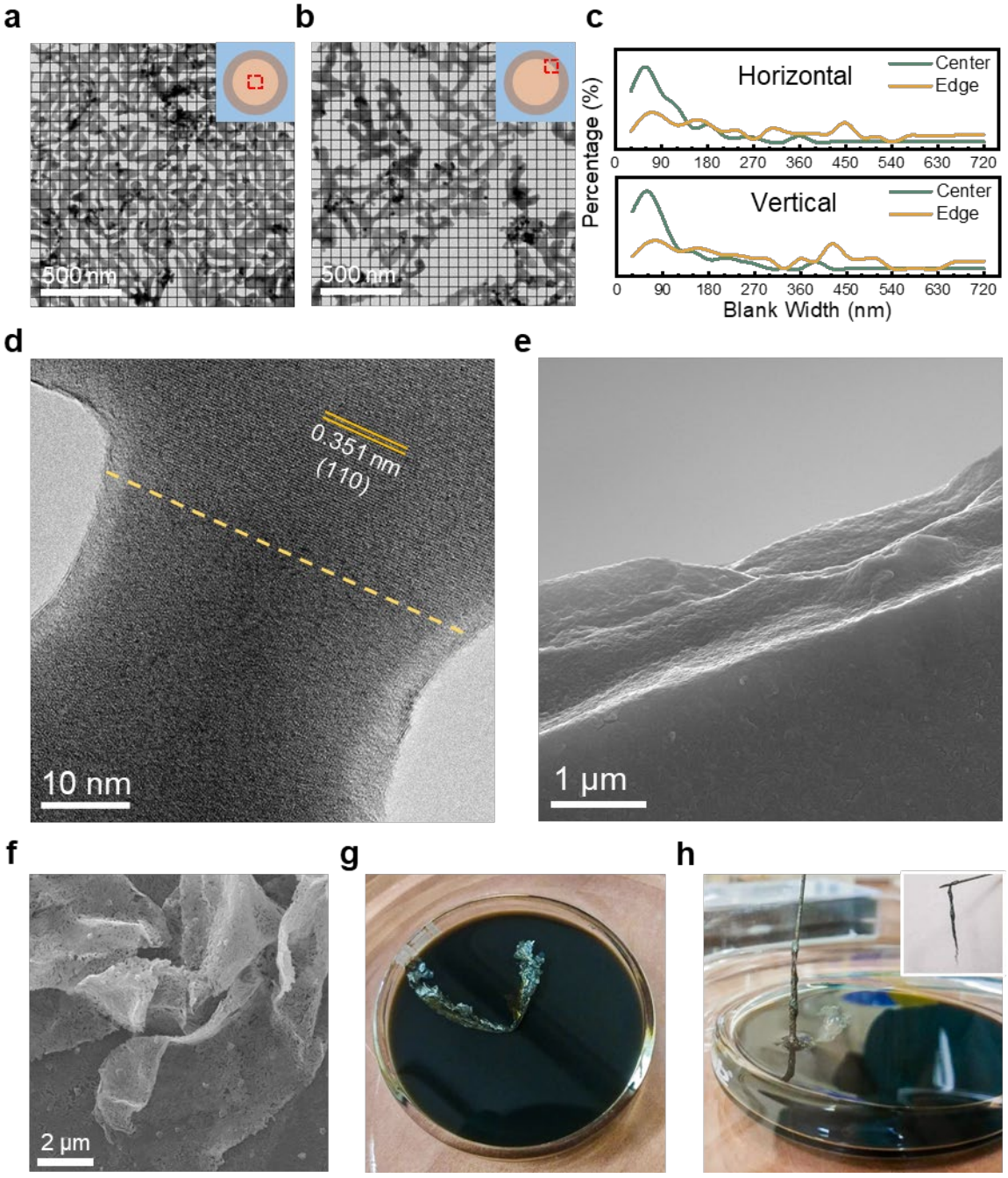

Figure 2. TEM image of Ag_2S nanomesh in different spots of the grid (shown in the insets): (a) in the centre and (b) on the edge. (c) Distributions of the blank widths along the horizontal and vertical direction of the grid. (d) HRTEM image of a ligament on the edge of the grid hole. (e) SEM image of Ag_2S membrane deposited on the broken face of a glass piece. (f) SEM image of wrinkled Ag_2S membrane. (g) Photo of a folded membrane after adding ethanol to the solution. (h) The folded membrane was picked out of the water with a needle.

The exceptional flexibility and foldability of the Ag_2S nanomesh membrane is first demonstrated by robust manipulations. For instance, the deposition can also be facilely realized on extremely rough surfaces, e.g. the breaking face of glass (Figure 2e). The membrane perfectly followed the complex topography without any breakage. This process reminds one of the stamping procedure in metal sheet processing,[16] whereas instead of using a machine for stamping pressing, the surface tension and atmospheric pressure naturally forced the membrane to adapt to the rough surface in our case. Another demonstration is that the membrane curled up owing to flow vibration during transfer (Figure 2f and Figure S10), similar to single-layer[10] or few-layer[15] 2D materials and some soft 2D polymers.[17] Next, a dynamic observation was made by adding a drop of ethanol into the solution. The membrane on the water surface was violently disturbed and folded into a scroll due to a sudden decrease of the surface tension (Figure 2g). The scroll can be picked up by a needle, overcoming the gravity and surface tension from the water. The excellent mechanical properties of the membrane endow it with a promising functional layer for flexible and wearable device fabrication as demonstrated below.

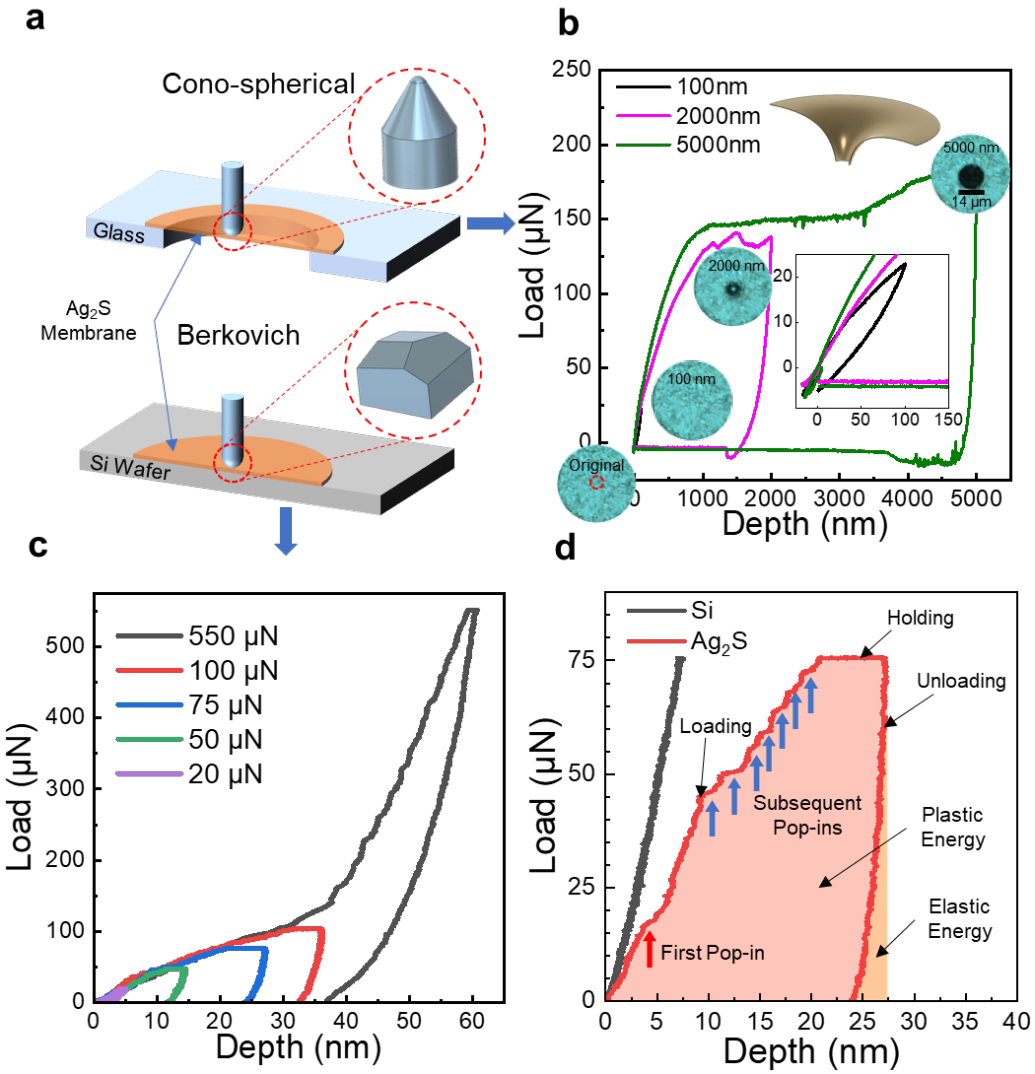

Figure 3. (a) Schematic illustration of nanoindentations with different indenter tips and substrates. Note the orange-colour Ag_2S membranes possess a nanomesh porous structure. (b) The typical load-depth curve of nanoindentation on Ag_2S membrane over a 50 μm hole. (c) The representative load-depth curves of nanoindentation tests on the Ag_2S membrane on a solid silicon wafer. (d) The representative load-depth curves of nanoindentation tests on the silicon wafer (black line) and Ag_2S membrane on a silicon wafer (red line) under the load of 75 μN.

To gain quantitative insights into the mechanical properties, the Ag_2S membrane was deposited over patterned holes (Φ50×40 μm, glass substrate) for nanoindentation tests (Figure 3a, top). The load-depth curve and the corresponding optical microscopic images of the membrane after each indentation were shown in Figure 3b. First, a 100 nm-depth indentation was applied to probe the mechanical response. The displacement returned to zero upon

unloading, indicating elastic behavior under such small displacement. When the indentation depth increased to 2000 nm, the load-depth curve can be divided into two stages: the steep increase stage from the beginning to 1140 nm displacement, followed by the second stage of a vibrant plateau. A circle rupture with a radius of ca. 8 μm was seen within the film, which should occur at the transition point (depth 1140 nm, load 113 μN) of the loading process. Careful observation reveals the smooth funnel-shaped rupture toward the bottom (inset in Figure 2b), confirming the exceptional deformability of the membrane. The following 5000 nm indentation demonstrates a similar mechanical response, although the membrane was already damaged after the 2000 nm indentation. The circular void was enlarged but still stayed localized, and no cracks were observed around it. These results imply that the membrane was highly tolerant for structural defects, and the stress was beard by the whole membrane upon large displacement. The break strength σ_{max} was estimated to be 741 MPa according to the equation $\sigma_{max}=(F_{max}E/4\pi r_{tip}t)^{1/2}$, where F_{max} is the maximum load before the break (113 μN in here), E is Young's modulus of the material, r_{tip} is the radius of the indenter tip, and t is the thickness of the film[10-11, 14-15, 18-19]. This value is much higher than the value of bulk Ag_2S (63.9 MPa). We propose three main reasons that may cause the high break strength: i) The strength was overestimated because of the ignored nonlinear elasticity in the equation above[11]; ii) Compared with the nanoindentation carried out on 2D materials, a blunter tip (r_{tip}/t is 10 times lower) was used and resulted in a higher breaking force which is sensitive to tip radius[11]; iii) The strength of materials normally is enhanced when the size decreases due to the size effect[20].

It has been recognized that micro/macro-porous structures can have a substantial impact on the mechanical properties of materials and can even change a rigid material to a flexible one.[21-22] In this context, it is necessary to determine if the intrinsic mechanical nature of the Ag_2S ligaments contributes to the flexibility of the nanomesh; in other words, to verify if the plasticity of bulk Ag_2S is maintained down to the nanoscale. In this regard, the membrane was

deposited on a solid silicon wafer for further nanoindentation test (Figure 3a, bottom). Upon fixed loads, (varying from 20 to 500 μN, Figure 3c) the hysteresis comprising loading, holding, and unloading stages indicates the plastic deformation upon the compressive stress[23]. The substrate effect became visible for the 550 μN load cycle as implied by the sudden force increase at 38 nm depth. Therefore, a more detailed analysis is conducted based on the 75 μN indentation curve (for comparison, the test on the bare silicon wafer is also recorded as the black line). During the early loading stage, the curve obeys the Hertz contact theory with a continuous deformation.[24] When the load reached a critical value (17.5 μN), the first pop-in (small horizontal plateau) occurred, followed by the second and more pop-ins across the loading stage. The pop-in discontinuities in the loading curve are strongly indicative of the plasticity of the membrane, as frequently observed in nanoindentation on metals where the pop-ins occur owing to dislocation nucleation and avalanches[24-26]. In terms of bulk Ag_2S, Shi *et al*. argued its high plasticity originates from the relatively weak Ag-S bond between the slip plane which results in easy slipping along the [001] direction[4]. Our results suggest that the plasticity is retained in the Ag_2S membrane with its thickness down to 50 nm, although the detailed mechanism for the pop-ins is under investigation. In this regard, the total work of the indentation U_t, the elastic work U_e, and the plastic work U_p under different loads (Figure S11) were calculated, where $U_t=U_e+U_p$. Under 75 μN load and 27.5 nm displacement, the U_t was calculated to be 1.3e-3 nJ, meaning up to 95% of the energy was dissipated in plastic deformation (U_p).

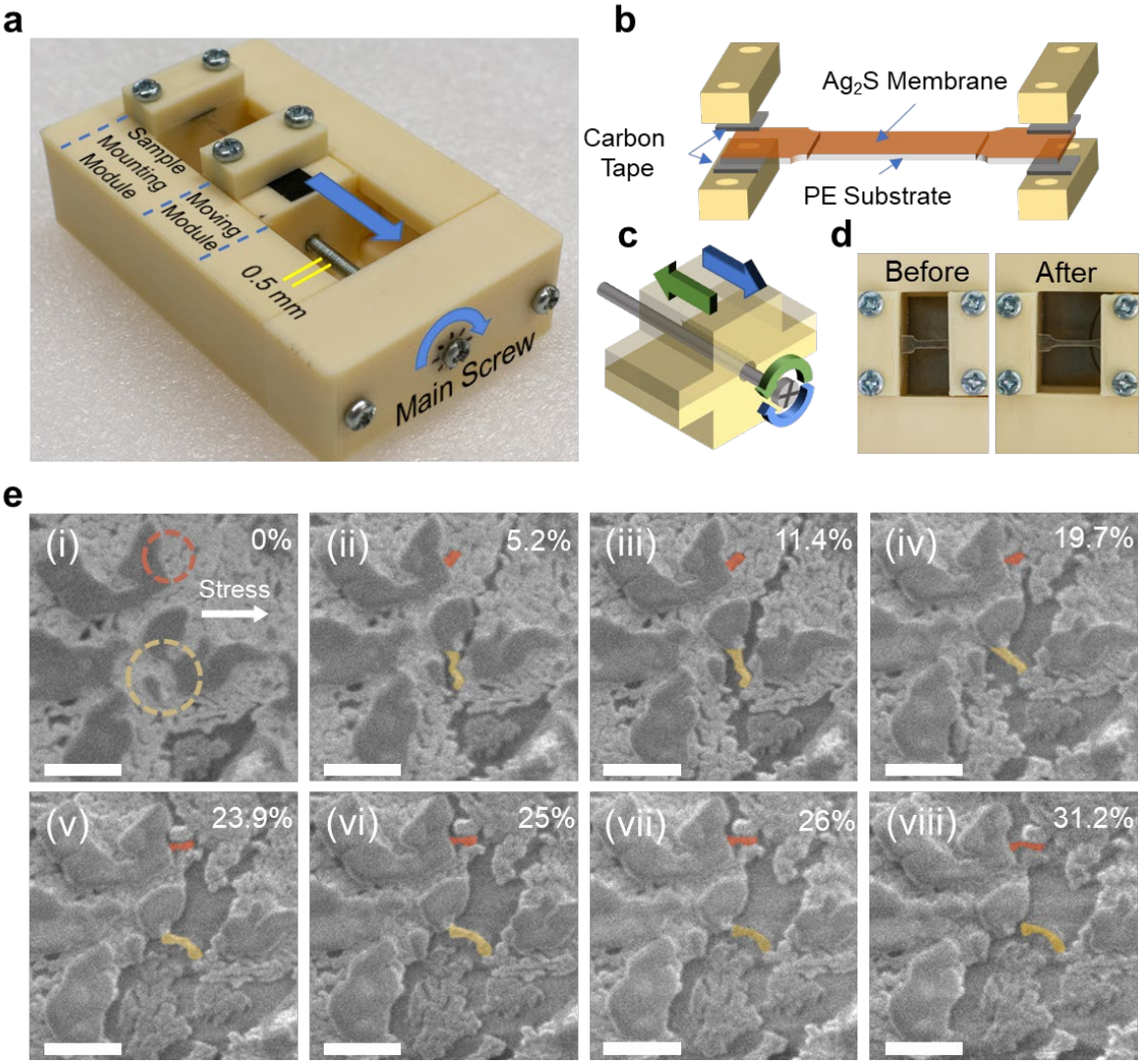

Figure 4. (a) Picture of the self-designed 3D printed stage for tensile test. (b) illustration of the method for mounting the substrate. The orange stripe is the dog-bone-shaped plastic substrate with Ag_2S membrane on top, and the grey ones are the carbon tapes for fixing the substrate. (c) Schematic illustration of the moving modules in the tensile test. (d) Top-view photo of the substrate before (left) and after (right) the tensile test. (e) SEM images of Ag_2S membrane during the tensile test under different strains. Scale bars 1μm.

To monitor the real-time behavior of individual ligaments during tensile deformation, a device for *pseudo*-in-situ tensile test under SEM (Supporting video) was home-designed and fabricated by 3D printing (process details in Figure S12). The Ag_2S membrane was deposited on a standard dog-bone-shaped polyethylene substrate and then mounted on the tensile stage (Figure 4a, b). The stress is applied to the polymer substrate by clockwise turning of the main

screw and the precision of strain is 1% (Figure 4c). Some flaws were present in the membrane (Figure 4e-i) due to the roughness of the substrate, which can just be used as landmarks for locating the target ligaments. Two ligaments became visible at 5.2% engineering strain and were selected to study the mechanical response against the horizontal stress (Figure 4e, ii). The orange-colored ligament had a length of 210 nm and a width of 150 nm at this stage, and obvious elongation was seen when the strain of the substrate reached 19.7%. The length increased by 133% and the width decreased by 40% under 31.2% strain (Figure 4e, iii-viii). The situation of the yellow-colored ligament response is a bit more complex. Firstly, the direction of this ligament was gradually changed from perpendicular to the stress to almost parallel to the stress (Figure 4e, ii-v). As the stress continued, necking occurred in the middle of the ligament (Figure 4e, vi-viii). Finally, the ligament was detached from the matrix on its left side, whereas no crack was observed within it. The *pseudo*-in-situ recorded elongation and necking phenomenon provide strong evidence of the plasticity of the Ag_2S ligaments in the nanomesh.

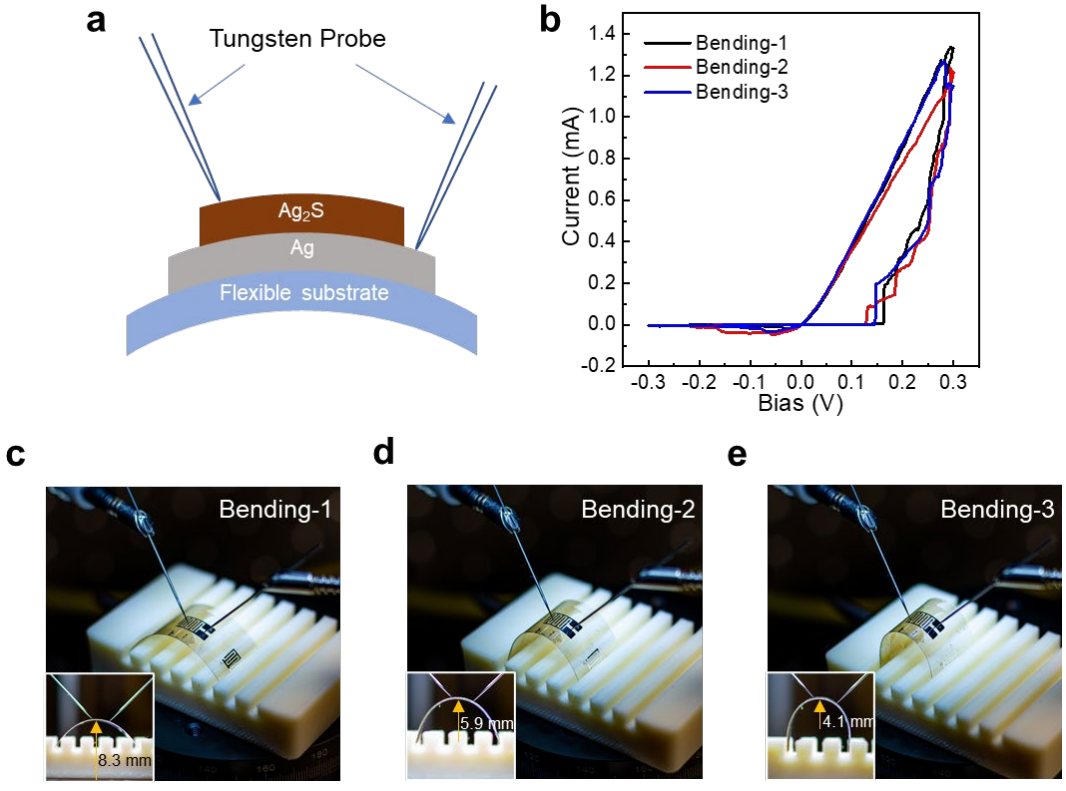

Figure 5. (a), Schematic illustration of the resistive switching device structure. (b), Current-bias curves of the device under different bending radii respond to (c)-(e). (c)-(e) Photos of the flexible Ag_2S device under electrical test with different bending radii. Insets show the side views of the device.

Resistance switching can occur in Ag_2S by applying an external electric field, transitioning from a high resistance state (HRS) to a low resistance state (LRS) due to the formation of Ag channels[27-28]. This property endows Ag_2S with the potential for developing next-generation non-volatile memory devices. Herein, a transparent flexible resistance-switching device was fabricated by depositing the membrane on a flexible polyethylene terephthalate (PET) substrate with silver electrodes as the bottom contact (Figure 5a). The current-voltage (I-V) characteristics were recorded with a probe station at different bending curvatures (Figure 5b), revealing the transition from the HRS (average resistance 82 kΩ) to LRS (average resistance 0.25 kΩ) when the bias reached 0.15 V (sweeping from 0-0.3 V). We note that the switching performance remained almost constant, even when the substrate was bent over 180° (Figure 5c-e and Figure S13).

In conclusion, Ag_2S nanomesh membrane with infinite lateral size was obtained via the one-step, self-regulated growth at the water-air interface. It is worth noting that the membrane can be renewably grown after it is transferred to substrates for measurements and device fabrication. Substantial flexibility, deformability and strength of the membrane were observed via macroscopic manipulation and nanoindentation tests. Nanoindentation also revealed the intrinsic plasticity of the ligaments within the membrane, as indicated by the pop-ins in the loading curve. The *pseudo*-in-situ tensile test under SEM was then performed on a home-made tensile stage to monitor the response of the ligaments under lateral stress, and the plasticity was further confirmed by the elongation and necking phenomena. Bendable resistive switching devices were fabricated based on the Ag_2S membrane. Low dimensional Ag_2S materials such as quantum dots and nanowires have been synthesized and applied for optoelectronics and

catalysis[29-31] and the presented Ag_2S nanomesh will be explored in these fields. In the future, wearable devices and multi-functional nanocomposite[32] with Ag_2S nanomesh as the active layer will be made accessible.

Methods

Ag_2S membrane preparation

In a typical process, amidinothiourea (ADT, Ourchem, 98%) and silver nitrate ($AgNO_3$, Chem-Supply, 99.5%) were dissolved in DI water (18.2 MΩ) with a concentration of 40 mM. After adding 10 mL ADT solution into a petri dish with a diameter of 6 cm, 10 mL $AgNO_3$ solution was added into the petri dish carefully and avoid violent disturbance and vortex. The petri dish with the mixed solution was put on a steady table without vibration and exposed to light for 24 h, and the membrane would be obtained at the interface.

Characterizations

The powder X-ray diffraction pattern was collected by Rigaku Smartlab diffractometer with a capillary tube (Φ 0.3 mm). Field-emission scanning electron microscopy (SEM, JEOL 7001f) was used to characterize the micro surface morphology of Ag_2S thin film on different substrates (such as glass, copper grid, silicon wafer, plastic) with no carbon/gold coating. Transmission electron microscopy (TEM) and high-res TEM (HRTEM) images were taken by JEOL 2100 under 200kV. The thickness and roughness of Ag_2S thin film were measured by atomic force microscopy (AFM, Bruker Dimension Icon) under contact mode. The data of particle size distribution was collected by Malvern Zetasizer Nano ZS.

Nanoindentation

The nanoindentation experiments were carried out by Hysitron TI 950 Tribonidenter. The nanoindentation was carried out under displacement-control mode with a cono-spherical indenter (tip diameter of 5 μm) when the membrane is on the hole (Figure 3b), and under load-control mode with a Berkovich indenter (tip diameter of 150 nm) when the membrane is on the silicon wafer (Figure 3c and 3d).

Pseudo-in-situ tensile test

The dog-bone-shaped plastic substrates for the *pseudo*-in-situ tensile test were cut off from a polyethylene film by laser. The device for the *pseudo*-in-situ tensile test under SEM was home-designed (Figure S12) and printed by a 3D printer with ABS plastic. The *pseudo*-in-situ tensile test was carried out under SEM (JEOL 7001f) with 1 kV and a working distance of 13 mm.

Resistive switching test

The resistive switching experiments were carried out on a probe station with two tungsten probes which are connected to Keithley 2636B system sourcemeter. The bottom interdigital silver electrodes were deposited on a flexible substrate through physical vapor deposition with a thickness of 150 nm. The Ag_2S membrane was then deposited on the substrate with the silver electrode through the method presented in Figure S3. The whole resistive switching tests were carried out on a stabilized platform in a dark laboratory, and the current-voltage (*I-V*) characteristics were recorded under a sweeping bias from -0.3 V to 0.3 V (-0.3 V → 0 V → 0.3 V → 0 V → -0.3 V) with a step of 0.002 V.

Associated content

Supporting Information

The Supporting Information is available free of charge at https://pubs.acs.org/

Additional bright-field and dark-field TEM images, powder XRD pattern, UV-Vis spectroscopy of Ag_2S membrane, detailed membrane deposition method, AFM topographic images of Ag_2S membrane formed with different time, photo of Ag_2S droplets with different sizes, photo of Ag_2S suspensions with different surfactants, TEM and HRTEM images of Ag_2S nanoparticles, blank width and connectivity distributions of Ag_2S membrane on grid, additional SEM images of Ag_2S membrane on different substrates, plasticity and elasticity energy ratios under different indentation depths, three-view drawing of tensile test device and schematic illustration of dog-bone-shape substrate, additional SEM image of Ag_2S membrane on a flexible substrate under bending state.

Author information

Corresponding Author

Jingsan Xu - School of Chemistry and Physics and Centre for Materials Science, Queensland University of Technology, Brisbane, Queensland 4000, Australia; Email: Jingsan.Xu@qut.edu.au

Authors

Yuting Wang - School of Chemistry and Physics and Centre for Materials Science, Queensland University of Technology, Brisbane, Queensland 4000, Australia

Wei Li - School of Chemistry and Physics and Centre for Materials Science, Queensland University of Technology, Brisbane, Queensland 4000, Australia

Yanan Xu - Central Analytical Research Facility, Institute for Future Environments, Queensland University of Technology, Brisbane, Queensland 4000, Australia

Chenhui Han - School of Chemistry and Physics and Centre for Materials Science, Queensland University of Technology, Brisbane, Queensland 4000, Australia

Peng Meng - School of Chemistry and Physics and Centre for Materials Science, Queensland University of Technology, Brisbane, Queensland 4000, Australia

Cheng Yan - School of Mechanical, Medical and Process Engineering, Queensland University of Technology, Brisbane, QLD 4000, Australia

Dongchen Qi - School of Chemistry and Physics and Centre for Materials Science, Queensland University of Technology, Brisbane, Queensland 4000, Australia

Acknowledgment

The authors acknowledge the financial support by the Australian Research Council. The faculty of Science and Central Analytical Research Facility (CARF) at QUT are greatly acknowledged for

technical assistance. We thank Dr. M. Johnston from the Faculty of Engineering for modelling and 3D printing of the tensile test stage.

References

1. Jo, S.; Cho, S.; Yang, U. J.; Hwang, G. S.; Baek, S.; Kim, S. H.; Heo, S. H.; Kim, J. Y.; Choi, M. K.; Son, J. S., Solution-Processed Stretchable Ag_2S Semiconductor Thin Films for Wearable Self-Powered Nonvolatile Memory. *Adv. Mater.* **2021,** *33* (23), 2100066.
2. Liu, L.; Li, T.; Ma, L.; Li, W.; Gao, S.; Sun, W.; Dong, R.; Zou, X.; Fan, D.; Shao, L.; Gu, C.; Dai, N.; Yu, Z.; Chen, X.; Tu, X.; Nie, Y.; Wang, P.; Wang, J.; Shi, Y.; Wang, X., Uniform Nucleation and Epitaxy of Bilayer Molybdenum Disulfide on Sapphire. *Nature* **2022,** *605* (7908), 69-75.
3. Raegen, A. N.; Yin, J.; Zhou, Q.; Forrest, J. A., Ultrastable Monodisperse Polymer Glass Formed by Physical Vapour Deposition. *Nat. Mater.* **2020,** *19* (10), 1110-1113.
4. Shi, X.; Chen, H.; Hao, F.; Liu, R.; Wang, T.; Qiu, P.; Burkhardt, U.; Grin, Y.; Chen, L., Room-temperature Ductile Inorganic Semiconductor. *Nat. Mater.* **2018,** *17* (5), 421-426.
5. Oshima, Y.; Nakamura, A.; Matsunaga, K., Extraordinary Plasticity of an Inorganic Semiconductor in Darkness. *Science* **2018,** *360* (6390), 772-774.
6. Wei, T.-R.; Jin, M.; Wang, Y.; Chen, H.; Gao, Z.; Zhao, K.; Qiu, P.; Shan, Z.; Jiang, J.; Li, R.; Chen, L.; He, J.; Shi, X., Exceptional Plasticity in the Bulk Single-crystalline van der Waals Semiconductor InSe. *Science* **2020,** *369* (6503), 542-545.
7. Lei, Y.; Gu, L.; Yang, X.; Lin, Y.; Zheng, Z., Ductile-Metal Ag as Buffer Layer for Flexible Self-powered Ag_2S Photodetectors. *Adv. Mater. Interfaces* **2021,** *8* (9), 2002255.
8. Yun, J., Ultrathin Metal films for Transparent Electrodes of Flexible Optoelectronic Devices. *Adv. Funct. Mater.* **2017,** *27* (18), 1606641.
9. Xue, X.; Penn, R. L.; Leite, E. R.; Huang, F.; Lin, Z., Crystal Growth by Oriented Attachment: Kinetic Models and Control Factors. *CrystEngComm* **2014,** *16* (8), 1419-1429.
10. Lee, G.-H.; Cooper, R. C.; An, S. J.; Lee, S.; Zande, A. v. d.; Petrone, N.; Hammerberg, A. G.; Lee, C.; Crawford, B.; Oliver, W.; Kysar, J. W.; Hone, J., High-Strength Chemical-Vapor-Deposited Graphene and Grain Boundaries. *Science* **2013,** *340* (6136), 1073-1076.
11. Lee, C.; Wei, X.; Kysar, J. W.; Hone, J., Measurement of the Elastic Properties and Intrinsic Strength of Monolayer Graphene. *Science* **2008,** *321* (5887), 385-388.
12. Liu, K.; Yan, Q.; Chen, M.; Fan, W.; Sun, Y.; Suh, J.; Fu, D.; Lee, S.; Zhou, J.; Tongay, S.; Ji, J.; Neaton, J. B.; Wu, J., Elastic Properties of Chemical-vapor-deposited Monolayer MoS_2, WS_2, and their Bilayer Heterostructures. *Nano Lett.* **2014,** *14* (9), 5097-103.
13. Castellanos-Gomez, A.; Poot, M.; Steele, G. A.; van der Zant, H. S.; Agrait, N.; Rubio-Bollinger, G., Elastic Properties of Freely Suspended MoS_2 Nanosheets. *Adv. Mater.* **2012,** *24* (6), 772-5.
14. Bertolazzi, S.; Brivio, J.; Kis, A., Stretching and Breaking of Ultrathin MoS_2. *ACS Nano* **2011,** *5* (12), 9703-9709.
15. Castellanos-Gomez, A.; Poot, M.; Amor-Amorós, A.; Steele, G. A.; van der Zant, H. S. J.; Agraït, N.; Rubio-Bollinger, G., Mechanical Properties of Freely Suspended Atomically Thin Dielectric Layers of Mica. *Nano Res.* **2012,** *5* (8), 550-557.
16. Lim, Y.; Ulsoy, A. G.; Venugopal, R., Process Control for Sheet-metal Stamping. *Springer*, 2013, 4-10.
17. Feng, X.; Schluter, A. D., Towards Macroscopic Crystalline 2D Polymers. *Angew. Chem. Int. Ed. Engl.* **2018,** *57* (42), 13748-13763.
18. Ruiz-Vargas, C. S.; Zhuang, H. L.; Huang, P. Y.; van der Zande, A. M.; Garg, S.; McEuen, P. L.; Muller, D. A.; Hennig, R. G.; Park, J., Softened Elastic Response and Unzipping in Chemical Vapor Deposition Graphene Membranes. *Nano Lett.* **2011,** *11* (6), 2259-63.
19. Song, L.; Ci, L.; Lu, H.; Sorokin, P. B.; Jin, C.; Ni, J.; Kvashnin, A. G.; Kvashnin, D. G.; Lou, J.; Yakobson, B. I.; Ajayan, P. M., Large Scale Growth and Characterization of Atomic Hexagonal Boron Nitride Layers. *Nano Lett.* **2010,** *10* (8), 3209-15.
20. Cheng, G.; Chang, T. H.; Qin, Q.; Huang, H.; Zhu, Y., Mechanical Properties of Silicon Carbide Nanowires: Effect of Size-dependent Defect Density. *Nano Lett.* **2014,** *14* (2), 754-8.
21. Blees, M. K.; Barnard, A. W.; Rose, P. A.; Roberts, S. P.; McGill, K. L.; Huang, P. Y.; Ruyack, A. R.; Kevek, J. W.; Kobrin, B.; Muller, D. A.; McEuen, P. L., Graphene Kirigami. *Nature* **2015,** *524* (7564), 204-7.

22. Guo, F.; Jiang, Y.; Xu, Z.; Xiao, Y.; Fang, B.; Liu, Y.; Gao, W.; Zhao, P.; Wang, H.; Gao, C., Highly Stretchable Carbon Aerogels. *Nat. Commun.* **2018,** *9* (1), 881.
23. Oyen, M. L.; Cook, R. F., A Practical Guide for Analysis of Nanoindentation Data. *J. Mech. Behav. Biomed. Mater.* **2009,** *2* (4), 396-407.
24. Sato, Y.; Shinzato, S.; Ohmura, T.; Hatano, T.; Ogata, S., Unique Universal Scaling in Nanoindentation Pop-ins. *Nat. Commun.* **2020,** *11* (1), 4177.
25. Pohl, F., Pop-in Behavior and Elastic-to-plastic Transition of Polycrystalline Pure Iron During Sharp Nanoindentation. *Sci. Rep.* **2019,** *9* (1), 15350.
26. Dimiduk, D. M.; Woodward, C.; LeSar, R.; Uchic, M. D., Scale-Free Intermittent Flow in Crystal Plasticity. *Science* **2006,** *312* (5777), 1188-1190.
27. Xu, Z.; Bando, Y.; Wang, W.; Bai, X.; Golberg, D., Real-time in situ HRTEM-resolved Resistance Switching of Ag_2S Nanoscale Ionic Conductor. *ACS Nano* **2010,** *4* (5), 2515-2522.
28. Waser, R.; Aono, M., Nanoionics-based Resistive Switching Memories. *Nanosci. Technol.*, 2007; Vol. 6, pp 833-840.
29. Sadovnikov, S. I.; Gusev, A. I., Recent Progress in Nanostructured Silver Sulfide: From Synthesis and Nonstoichiometry to Properties. *J. Mater. Chem. A* **2017,** *5* (34), 17676-17704.
30. Liu, S.; Tao, H.; Liu, Q.; Xu, Z.; Liu, Q.; Luo, J.-L., Rational Design of Silver Sulfide Nanowires for Efficient CO_2 Electroreduction in Ionic Liquid. *ACS Catal.* **2018,** *8* (2), 1469-1475.
31. Ren, Z.; Shen, C.; Yuan, K.; You, J.; Li, N.; Xie, K., Synthesis of Silver Sulfide Nanowires: Variation of the Morphology and Structure. *Mater. Today Commun.* **2022,** *31,* 103917.
32. Zhao, X. F.; Yang, S. Q.; Wen, X. H.; Huang, Q. W.; Qiu, P. F.; Wei, T. R.; Zhang, H.; Wang, J. C.; Zhang, D. W.; Shi, X.; Lu, H. L., A Fully Flexible Intelligent Thermal Touch Panel Based on Intrinsically Plastic Ag_2S Semiconductor. *Adv. Mater.* **2022,** *34* (13), 2107479.

For Table of Contents Only